INTERNATIONAL JOURNAL FOR NUMERICAL METHODS IN FLUIDS
Int. J. Numer. Meth. Fluids 2004; **46**:203–226 (DOI: 10.1002/fld.757)

A finite element model for the simulation of lost foam casting

G. Houzeaux*,† and R. Codina‡

CIMNE, Edificio C1, Campus Nord UPC, Gran Capità s/n, 08034 Barcelona, Spain

SUMMARY

In this paper, we present a numerical model to simulate the lost foam casting process. We introduce this particular casting first in order to capture the different physical processes in play during a casting. We briefly comment on the possible physical and numerical models used to envisage the numerical simulation. Next we present a model which aims to solve 'part of' the complexities of the casting, together with a simple energy budget that enables us to obtain an equation for the velocity of the metal front advance. Once the physical model is established we develop a finite element method to solve the governing equations. The numerical and physical methodologies are then validated through the solution of a two- and a three-dimensional example. Finally, we discuss briefly some possible improvements of the numerical model in order to capture more physical phenomena. Copyright © 2004 John Wiley & Sons, Ltd.

KEY WORDS: lost foam casting; simulation; finite element method; ALE method

1. INTRODUCTION

In this paper we present a numerical model for the simulation of a relatively new casting process, known as lost foam casting (LFC) or evaporative pattern casting (EPC). See Reference [1] for an introduction to LFC. This process was developed during the sixties and has experienced an exponential growth since then. To illustrate the importance gained by this technology in the last years, let us mention that around 20% of the total aluminium casting in the U.S. is obtained by LFC [2]. Despite its important place on the casting market, it is only recently that numerical codes have allowed the numerical simulation of LFC. This is partly due to the complexity of the physical processes in play.

In general castings, known as Gravity Casting, the molten metal is poured into a mold filled with air. The metal is allowed to fill the mold due to gravity, as long as the pressure at

*Correspondence to: G. Houzeaux, CIMNE, Edificio C1, Campus Nord UPC, Gran capità s/n, 08034 Barcelona, Spain.
†E-mail: houzeaux@cimne.upc.es
‡E-mail: ramon.codina@upc.es

Contract/grant sponsor: European Project FOAMCAST; contract/grant number: G1RD-CT-2000-00417

Published online 14 July 2004

Received 10 October 2003
Revised 30 April 2004

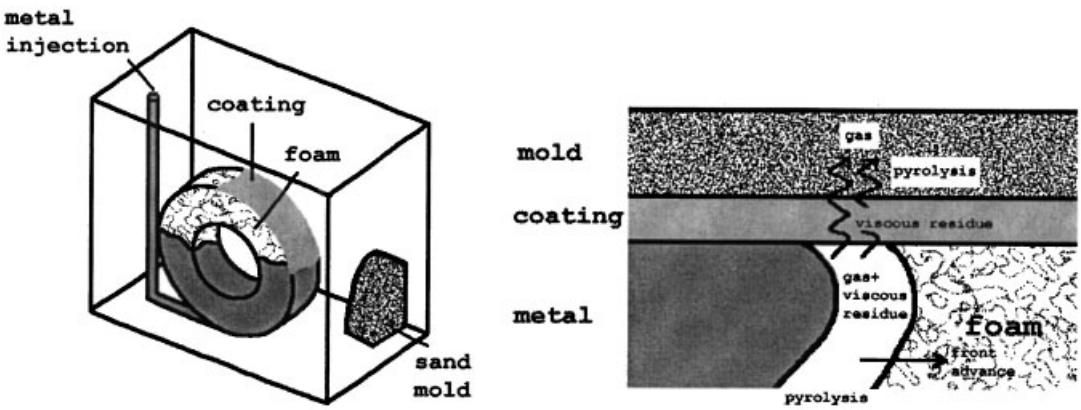

Figure 1. LFC. (Left) Main components. (Right) Main physical processes in play.

the inflow is sufficiently high. In LFC, the air is replaced by expandable polystyrene (EPS). The polystyrene bead is placed in the mold, is heated and expands until it completely fills the mold. The resulting cluster is dipped into a permeable refractory coating (of alumina, silica e.g.) which act as a barrier between the sand and the metal, providing a control on the escape of gases and a better surface finish. It is then embedded in a container filled with compacted sand and provided with a gating. See the sketch in Figure 1 (Left).

LFC casting operates as follows. The molten metal is poured into the gating and once it comes into contact with the foam, the foam evaporates; this process is known as pyrolysis. Gases can vent through the sand if the coating is sufficiently permeable. However, if the gas is not vented sufficiently fast, casting defects can appear and perturb the metal advance. Figure 1 (Right) shows a simplified scheme of a casting using the lost foam technique. The main parameters that control the process are the EPS pattern and the combustion characteristics, the coating material, thickness, texture and permeability.

LFC presents many advantages over other methods such as green sand or die castings. From the practical point of view, it simplifies the casting process and enables the manufacturing of complex shapes without the need for cores, which are useful in classical casting to produce holes or passages. LFC provides tight-dimensional tolerances, smooth surface finish and does not present parting lines (the lines which separate a mold into several parts). It therefore enable the reduction of the machining costs and the save on energy costs are higher than 30% with respect to standard castings.

The numerical approach to LFC casting requires special attention at the physical and the numerical level. Due to the complex physical mechanisms involved, some physical simplifications are needed. For example, we decide not to solve for the combustion of the foam. Instead, we obtain an equation for the metal front velocity, through a simple energy budget. Neither do we consider the coating, although its effects can be taken into account in the equation for the front velocity. The foam is assumed to be burnt instantaneously, and the possible generation of viscous residues or defects is not considered [3]. A non-exhaustive list of the main assumptions is given in Section 1. LFC usually involves characteristic velocities lower than those encountered in classical casting and the metal flow can be either

laminar or turbulent. We have chosen a turbulence model which is able to predict the transition from the laminar to the turbulent state, namely the Spalart–Allmaras (SA) turbulence model which consists of one additional partial differential equation. However, in the examples presented in Section 3, the flows are considered fully turbulent and transition is not envisaged.

The velocity approach to treat the front advance is not the only possible. An alternative consists in prescribing the pressure at the front. This approach has the advantage that it naturally takes into account the back-pressure effects due to the decomposition of the EPS pattern. A possible implementation is explained in Reference [4]; this method however does not consider the heat transfer rate between metal and foam as explicit part of the front advance mechanism. See also Reference [5], where the authors propose in addition a model for the back-pressure.

The numerical approximation chosen to solve the present problem is the finite element method. In order to capture the ever changing computational domain occupied by the metal, three main approaches are available [6]. The first method consists in writing the governing equations in a Lagrangian frame of reference, the nodes being advected by the flow velocity [7, 8]. The second method is based on an Eulerian formulation. The position of the front is identified by a level set function [9], which is transported by the velocity [10, 11]. The third method is the Arbitrary–Lagrangian Eulerian (ALE) method, which uses both Lagrangian and Eulerian approaches, and consists in adapting the mesh to each new configuration but in limited zones; generally this implies a node movement near the front and a remeshing if the resulting mesh is too distorted [12, 13]. Let us mention finally the promising meshless method [14] used to solve free surface flows using a Lagrangian formulation. In this work we have chosen an ALE method, but with the originality that it is applied to a fixed mesh (FMALE). It will be described in Section 3.3.

2. PHYSICAL MODEL

2.1. Simplifying assumption

We described in Section 1 the complexity of the physical processes involved in LFC. In order to treat LFC numerically, some simplifying assumptions are needed. In addition, assumptions are added for the sake of clarity of the exposition. They are:

1. The metal and foam properties are constant (at least locally).
2. There is no solidification during filling.
3. There are no sources of contamination, like viscous residues. A simple equation to take into account the generation of contaminants will be given in Appendix B.
4. The foam is assumed to be a constant temperature obstacle so that no partial differential equation for the foam is, in principle, needed.
5. All the combustion gases escape through the coating and the mold. Therefore, no gas is trapped between the metal and the foam.

Using these simplifications, we are able to devise a concise physical model which is presented below.

2.2. Governing equations

Let Ω_{m} the domain that is filled by the molten metal, Ω_{f} be the domain occupied by the foam and Ω be the total domain (metal+foam). They are shown in Figure 2. Obviously, both domains depend on time.

Let us denote the physical properties as follows: ρ as the density, v as the kinematic viscosity, c_p as the specific heat at constant pressure, κ as the thermal diffusion coefficient and α_{ij} as the heat transfer coefficient between materials i and j. We introduce the kinematic pressure $p = P/\rho$ where P is the mechanical pressure. The unknowns to be determined in the general case are $\mathbf{u}$ the velocity, p the pressure and T the temperature of the molten metal. Let us denote u_{mf} as the velocity at which the front of molten metal advances through the foam.

The subscripts m, f and o will be used to refer to the physical properties of the molten metal, foam and mold, respectively. Likewise, Γ_{ij} will be used to denote the interface between materials i and j, and the subscript inf will refer to values at the inflow of the domain; see Figure 2.

The equations describing the lost foam model in an Eulerian frame of reference are the following:

$$\begin{aligned} \partial_t \mathbf{u} + (\mathbf{u}_a \cdot \nabla)\mathbf{u} - 2\nabla \cdot [v_{\mathrm{m}} \boldsymbol{\varepsilon}(\mathbf{u})] + \nabla p = 0 \\ \nabla \cdot \mathbf{u} = 0 \\ \partial_t T + \mathbf{u}_a \cdot \nabla T - \nabla \cdot (\kappa_{\mathrm{m}} \nabla T) = 0 \end{aligned}$$

to be solved in Ω_{m}, where $\boldsymbol{\varepsilon}(\mathbf{u})$ is the rate of deformation tensor given by

$$\boldsymbol{\varepsilon}(\mathbf{u}) = \tfrac{1}{2}(\nabla \mathbf{u} + \nabla \mathbf{u}^t)$$

We note that the advection velocity of the momentum and beat equations should be corrected from $\mathbf{u}$ to $\mathbf{u}_a$ as the domain Ω_{m} is moving; this point will be treated in Section 3.3. Likewise, the kinematic viscosity v_{m} and the diffusivity κ_{m} could be modified if a turbulence model is

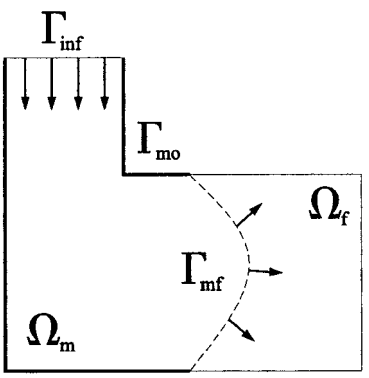

Figure 2. Domain and boundary notation.

used. The governing set of equations must be provided with initial and boundary conditions, the latter ones being:

$$\begin{aligned}
\boldsymbol{\sigma}\cdot\mathbf{n} &= -p_{\mathrm{inf}}\mathbf{n} \quad \text{on } \Gamma_{\mathrm{inf}}\\
\boldsymbol{\sigma}\cdot\mathbf{n}-(\mathbf{n}\cdot\boldsymbol{\sigma}\cdot\mathbf{n})\mathbf{n} &= 0,\\
\mathbf{u}\cdot\mathbf{n} &= \mathbf{0} \quad \text{on } \Gamma_{\mathrm{mo}}\\
\mathbf{u} &= \mathbf{u}_{\mathrm{mf}} \quad \text{on } \Gamma_{\mathrm{mf}}\\
T &= T_{\mathrm{inf}} \quad \text{on } \Gamma_{\mathrm{inf}}\\
-\kappa_{\mathrm{m}}\nabla T\cdot\mathbf{n} &= \alpha_{\mathrm{mo}}(T-T_{\mathrm{o}})/(\rho_{\mathrm{m}}c_{p\mathrm{m}}) \quad \text{on } \Gamma_{\mathrm{mo}}\\
-\kappa_{\mathrm{m}}\nabla T\cdot\mathbf{n} &= \alpha_{\mathrm{mf}}(T-T_{\mathrm{f}})/(\rho_{\mathrm{m}}c_{p\mathrm{m}}) \quad \text{on } \Gamma_{\mathrm{mf}}
\end{aligned} \tag{1}$$

The vector $\mathbf{n}$ is the outward unit normal to domain Ω_{m}, the tensor $\boldsymbol{\sigma}$ is the stress tensor given by

$$\boldsymbol{\sigma} = -p\mathbf{I} + 2\nu_{\mathrm{m}}\boldsymbol{\varepsilon}(\mathbf{u})$$

$\mathbf{I}$ being the n_d-dimensional identity. T_{inf} is the pouring temperature and p_{inf} is the pouring pressure. We note that the boundary condition given by Equation $(1)_1$ at the inflow is

$$p = p_{\mathrm{inf}} \quad \text{on } \Gamma_{\mathrm{inf}}$$

only if $\boldsymbol{\varepsilon}(u) = 0$, which is satisfied, for example if the flow is uniform. Equation $(1)_2$ is a slip condition that is usually used in mold filling simulations. It can be substituted by a no-slip condition.

In the governing set of equations, apart from the velocity, pressure and temperature, we are left with two unknowns, namely the front advance velocity and the time-dependent domain Ω_{m}. A model for the front advance velocity is now given. Following this model, a front advance tracking is presented to tackle the evolution of Ω_{m}. Finally, to close the physical description of the problem, we end up with the description of the turbulence model and the associated treatment for the wall boundary conditions.

2.3. *Front velocity*

The velocity at which the front advances is a function of the heat absorbed by the foam, which in turn depends on $\mathbf{u}$ and T so that $u_{\mathrm{mf}} = u_{\mathrm{mf}}(\mathbf{u}, T)$. If this heat is high enough, the foam will be molten and vaporized, and the space left free will be occupied by the metal. The front velocity can be computed using a simple global balance of energy. Suppose that a point at the interface of molten metal–foam advances a distance δs normal to the surface of the interface in a time δt. The heat per unit surface released from the molten metal to the volume initially occupied by foam will be

$$Q_{\mathrm{rel}} = \alpha_{\mathrm{mf}}(T_{\mathrm{m}} - T_{\mathrm{f}})\delta_t$$

This heat will be invested in melting and vaporizing the foam and in increasing the temperature of the spatial points, which originally are occupied by foam and at the end of the process are

filled with metal. Therefore, the heat stored can be approximated by

$$Q_{\text{sto}} = \left[\rho_{\text{f}} c_{p\text{f}} \frac{1}{\delta t} (T_{\text{m}} - T_{\text{f}}) + \frac{\rho_{\text{f}}}{\delta t} (E_{\text{mel}} + E_{\text{vap}}) \right] \delta s \delta t$$

where E_{mel} and E_{vap} are the melting and vaporization energy, respectively, which must be determined from experiments. Imposing that $Q_{\text{sto}} = Q_{\text{rel}}$ it is found that

$$\rho_{\text{f}} c_{p\text{f}} \frac{\delta s}{\delta t} (T_{\text{m}} - T_{\text{f}}) + \frac{\delta s}{\delta t} (\rho_{\text{f}} E_{\text{mel}} + \rho_{\text{f}} E_{\text{vap}}) = \alpha_{\text{mf}} (T_{\text{m}} - T_{\text{f}})$$

For $\delta t \to 0$, $\delta s / \delta t \to u_{\text{mf}}$, from where

$$u_{\text{mf}} = \frac{\alpha_{\text{mf}} (T_{\text{m}} - T_{\text{f}})}{\rho_{\text{f}} (c_{p\text{f}} (T_{\text{m}} - T_{\text{f}}) + E_{\text{mel}} + E_{\text{vap}})} \tag{2}$$

We note that the model for the front velocity does not take into account the effects of pouring temperature, coating, foam type, gravity, etc. In fact, the front velocity is independent on the mold orientation with respect to the gravity. From experiments, the front advance should depend on:

- The pouring temperature. The back-pressure due to the combustion of the foam increases with this temperature. For very high temperatures, the front velocity decreases with increasing pouring temperature. See for example the experiments carried out in References [15, 16]. In the first reference mentioned, the filling time of the plate solved in Section 4.1 goes from 2.1 to 3.5 s for temperature ranging from 490 to 1115°C.
- The coating. The type of coating determines the flow of the evacuation of the gas. For a high permeable coating, it is observed that the front velocity increases linearly with the pouring temperature [15]. For a given temperature, filling times can double according to the type of coating used.
- The foam. In Reference [17], the authors perform a multi-parameter experimental analysis to study the combined effects of foam material, coating, pouring temperature, etc. They show that the foam material is of primary importance in foam castings. In particular, they compare expendable polystyrene (EPS) and polymethyl methacrylate (PMMA). Even though these materials have similar densities, their chemical compositions and thermal decomposition characteristics are different so that they produce very different filling times (up to three times higher for PMMA). For example, EPS yields more viscous residue than PMMA; see Figure 1 (Right).
- Gravity. Although gravity **g** has no as strong effects as in empty cavity casting, in a lost foam process it can help to counterbalance the back-pressure. In Reference [16], a filling time of 2.7 s is obtained for a bottom gating (counter gravity), while a filling time of 1.75 s is obtained for a top gating.

In addition, more drastic effects can occur. For high temperatures and low coating permeabilities, a large gap between the front and the burnt foam is observed. This situation is not envisaged in the context of this work.

We now present a simple way to take into account the effects of the back-pressure p_{gas}. This is a first step in the improvement of the model. As we do not have at hand a combustion model, a formula for the back-pressure must be obtained from experimental results. According

to the previous remarks, we assume that

$$p_{\text{gas}} = p_{\text{gas}}(T_{\text{inf}}, \text{foam}, \text{coating}) \tag{3}$$

is a known function.

The second step consists in devising an expression for the metal-to-foam heat transfer coefficient by making explicit its dependence on p_{gas}. We assume that the heat transfer coefficient in the absence of back-pressure and gravity effects is known, and it is referred to as α^0_{mf}. It can be shown that the value of the heat transfer between two materials is proportional to their separation distance d. If we assume next that this distance is proportional to the pressure difference between the metal and the gas, we can then express the heat transfer as a function of these pressures. In particular, we have

$$\begin{aligned} p &= p_{\text{gas}} \rightarrow d = d_0 \rightarrow \alpha_{\text{mf}} = \alpha^0_{\text{mf}} \\ p &> p_{\text{gas}} \rightarrow d < d_0 \rightarrow \alpha_{\text{mf}} > \alpha^0_{\text{mf}} \\ p &< p_{\text{gas}} \rightarrow d > d_0 \rightarrow \alpha_{\text{mf}} < \alpha^0_{\text{mf}} \end{aligned}$$

From these remarks, we can derive an expression for the heat transfer coefficient, similar to that used in usual thermal contact models (See Reference [18]). We propose the following expression:

$$\alpha_{\text{mf}} := \alpha^0_{\text{mf}} \left(\frac{p}{p_{\text{gas}}} \right)^{\varepsilon} \tag{4}$$

This formula enables us to include in a simple way the effects of the set of parameters $(T_{\text{inf}}, \text{foam}, \text{coating}, \mathbf{g})$ in the determination of the front advance, as the front velocity u_{mf} depends explicitly on the heat transfer coefficient. Indeed, we have assumed that we knew an expression for the gas pressure in function of the pouring temperature, the foam and the coating, given by Equation (3). The dependence on gravity appears implicitly through the dependence on the pressure in Equation (4). We have therefore

$$u_{\text{mf}} = \frac{\alpha_{\text{mf}}(T_{\text{inf}}, \text{foam}, \text{coating}, \mathbf{g})(T_{\text{m}} - T_{\text{f}})}{\rho_{\text{f}}[c_{pf}(T_{\text{m}} - T_{\text{f}}) + E_{\text{mel}} + E_{\text{vap}}]}$$

This model is put to the test in Reference [19].

2.4. Front tracking

One possibility for defining the molten metal–foam interface (or equivalently to determine Ω_{m} at each time step) is the level set technique. This is not a general conservation law, but rather a mathematical model to describe the evolution of this interface (see Reference [10] for an application of this method to classical mould fillings). It consists in defining a scalar function, called the level set function (LSF), say ψ, over the computational domain Ω in such a manner that its value at a certain point indicates the presence or absence of metal. This function may be considered a fictitious fluid property. For instance, we may assign the value 1 to regions where the liquid metal has already entered and the value 0 to foam-filled regions. The position of the metal front will be defined by the isovalue contour $\psi = \psi_c$ where $\psi_c \in [0, 1]$ is a critical

value defined *a priori*. We usually take $\psi_c = 0.5$. This value is immaterial if ψ is a true step function, but is needed in the finite element discretization. The level set technique is usually used to follow the free surfaces of fluids, i.e. surfaces advected by the fluid velocity itself, like many other methods to track free surfaces such as the particle-in-cell technique or different variants of marker methods [20]. In the present case we have a somewhat different situation. The LSF is advected due to temperature gradients and is therefore not explicitly advected by the fluid motion (Equation (2)). The fluid motion is induced by the front advance and we can define formally:

$$\Omega_{\mathrm{m}} = \{\mathbf{x} \in \Omega \mid \psi(\mathbf{x}) \geqslant \psi_{\mathrm{c}}\}$$

In order to follow the motion of the front, a level set equation is solved in the following way:

$$\frac{\partial \psi}{\partial t} + \mathbf{u} \cdot \nabla \psi = 0 \tag{5}$$

where $\mathbf{u}$ is the velocity of the metal. Remember that at the metal–foam interface, the velocity is imposed as a Dirichlet boundary condition given by Equation $(1)_3$. The algorithm that allows us to correctly advect the LSF will be presented in Section 3.2, as its implementation is completely dependent on the numerical strategy presented in Section 3, namely the finite element method. Equation (5) must be provided with initial and boundary conditions. For example:

$$\psi = 1 \quad \text{on } \Gamma_{\mathrm{inf}}$$

In the latter section we derived an equation for the front velocity module. We now assume that the front is moving along the normal to the front, which is precisely the gradient of the level set function:

$$\mathbf{u}_{\mathrm{mf}} = -\frac{\nabla \psi}{|\nabla \psi|} \mathbf{u}_{\mathrm{mf}} \tag{6}$$

Another possibility would consist in assuming that the velocity is parallel to the temperature gradient such that

$$\mathbf{u}_{\mathrm{mf}} = -\frac{\nabla T}{|\nabla T|} \mathbf{u}_{\mathrm{mf}}$$

This option is not envisaged in this work.

2.5. Turbulence model

Turbulence is treated using the ensemble-averaging approach together with the Boussinesq approximation for the Reynolds stress tensor, and a similar apparent diffusion concept for the heat equation. The resulting system is referred to as the Reynolds-averaged Navier–Stokes (RANS) equations and reads:

$$\begin{aligned} \partial_t \mathbf{u} + (\mathbf{u}_a \cdot \nabla)\mathbf{u} - 2\nabla \cdot [(\nu_{\mathrm{m}} + \nu_t)\boldsymbol{\varepsilon}(\mathbf{u})] + \nabla p &= 0 \\ \nabla \cdot \mathbf{u} &= 0 \\ \partial_t T + \mathbf{u}_a \cdot \nabla T - \nabla \cdot [(\kappa_{\mathrm{m}} + \kappa_t)\nabla T] &= 0 \end{aligned}$$

where ν_t is the eddy viscosity (also referred to as apparent or turbulent viscosity), and κ_t is the turbulent diffusivity.

The turbulence model chosen to compute the eddy viscosity is the Spalart–Allmaras turbulence model. This model was devised 'using empiricism and arguments of dimensional analysis, Galilean invariance, and selective dependence on molecular viscosity' [21]. It consists of a transport equation for the eddy viscosity ν_t. For any details on the equation, see the original publication of the authors [21]. The transport equation for ν_t is

$$\partial_t \nu_t + \mathbf{u} \cdot \nabla \nu_t - c_{b_1} S \nu_t - \frac{1}{\sigma} [\nabla \cdot (\nu_t \nabla \nu_t) + c_{b_2} (\nabla \nu_t)^2] + c_{w_1} f_w \frac{\nu_t^2}{d^2} = 0$$

where c_{b_1}, c_{b_2}, σ and c_{w_1} are constants, S is the norm of the vorticity, f_w is a function depending on S, ν_t and the distance to the wall d. This equation is the high Reynolds number version of the model. Additional corrections enable the computation of low Reynolds number and transition effects, which not shown here for the sake of brevity.

The turbulent diffusivity is calculated through the introduction of the turbulent Prandtl number Pr_t defined as:

$$\kappa_t = \frac{\nu_t}{Pr_t} \tag{7}$$

In order to close the system of governing equations, an expression for Pr_t is needed. In general, we have that:

$$\text{For liquid metals: } Pr \ll 1, \quad Pr_t > 1, \quad Pr_t = Pr_t(Pr, Re, y)$$

where Re is the Reynolds number and y is the distance to the wall [22, 23]. The turbulent Prandtl number increases with decreasing Prandtl and Reynolds numbers. In Reference [24] the authors mention that *both theory and experiment suggest that* $Pr_t \to Pr_{t\infty}$, *a value common to all Pr, as* $Re \to \infty$. They derive an expression for the turbulent Prandtl number in pipe and channel flows with $Pr_{t\infty} = 0.85$. This is the value chosen in the present work. The system of governing equations is now closed.

2.6. Wall function approach

The RANS and turbulence equations are solved using the wall function approach [25] on the wall-type boundaries of the computational domain, i.e. Γ_{mo} in the present case. In order to avoid solving for the large gradients present in the boundary layer, the wall function approach implemented here consists in assuming that the computational wall is located at a distance y sufficiently far from the real wall where the no-slip condition for the velocity holds. Then the wall friction U_* is estimated by applying the law of the wall at y, i.e. by solving the non-linear Reichardt's law given by (see for example Reference [26]):

$$U^+ := \frac{U}{U_*} = \frac{1}{\chi} \ln(1 + \chi y^+) + 7.8 \left[1 - \exp\left(-\frac{y^+}{11} \right) - \frac{y^+}{11} \exp(-0.33 y^+) \right] \tag{8}$$

where U is the velocity at the computational wall, $\chi = 0.41$ is the Von Karman constant and where y^+ is the dimensionless distance to the wall of the boundary point defined as

$$y^+ := \frac{y U_*}{\nu_{\text{m}}}$$

The wall boundary condition for the momentum equations consists of a mixed Dirichlet/Neumann condition where the normal component of the velocity is zero and where the tangential component of the traction $\mathbf{t}$ is given by

$$\mathbf{t} = -U_*^2 \frac{\mathbf{u}}{|\mathbf{u}|}$$

Equation $(1)_2$ is therefore substituted by:

$$\mathbf{u}\cdot\mathbf{n} = 0, \quad \boldsymbol{\sigma}\cdot\mathbf{n} - (\mathbf{n}\cdot\boldsymbol{\sigma}\cdot\mathbf{n})\mathbf{n} = \mathbf{t}$$

The wall condition for the eddy viscosity is computed using the classical mixing length hypothesis together with the Van–Driest damping function, i.e. we impose that

$$\begin{aligned} \nu_t &= l_{\text{mix}}^2 \left|\frac{\mathrm{d}U}{\mathrm{d}y}\right| \\ l_{\text{mix}} &= \chi y^+ \left[1 - \exp\left(-\frac{y^+}{26}\right)\right] \end{aligned} \tag{9}$$

where $\mathrm{d}U/\mathrm{d}y$ is the normal derivative of the tangential velocity. Equation (9) corresponds to the inner-layer equation of the Baldwin–Lomax model, approximating the magnitude of the vorticity by $\mathrm{d}U/\mathrm{d}y$. It can be re-expressed in terms of the dimensionless quantities as:

$$\nu_t^+ = \chi^2 (y^+)^2 \left[1 - \exp\left(-\frac{y^+}{26}\right)\right]^2 \frac{\mathrm{d}U^+}{\mathrm{d}y^+}, \quad \nu_t^+ = \frac{\nu_t}{\nu_{\text{m}}}$$

where $\mathrm{d}U^+/\mathrm{d}y^+$ is obtained by simply deriving Reichardt's law (8), i.e.

$$\frac{\mathrm{d}U^+}{\mathrm{d}y^+} = \frac{1}{1+\chi y^+} + \frac{7.8}{11}\left[\exp\left(\frac{-y^+}{11}\right) + (0.33y^+ - 1)\exp(-0.33y^+)\right]$$

In the present work, we leave the wall boundary condition for the temperature unchanged although the heat transfer coefficient may be different in the turbulent case.

3. NUMERICAL MODEL

In the previous section we presented the physical modeling of the lost foam process. However, some purely numerical ingredients are necessary to solve the governing equations efficiently. We first introduce the finite element method which is used to solve the partial differential equations. Next we introduce the treatment of the front advance. Then we explain how this method affects the governing equations; in particular we will see that it can be viewed as an arbitrary Lagrangian (ALE) method applied to fixed meshes. Then we explain the complete numerical algorithm.

3.1. Finite element method and time discretization

The RANS, heat and SA equations are solved using a Finite Element model based on a stabilized Galerkin method. It is well-known that the Galerkin formulation can lack stability

for two major reasons. The first reason is related to the compatibility of the finite element spaces for the velocity and the pressure which have to satisfy the so-called Ladyzhenskaya–Brezzi–Babuška (LBB) condition. This condition is necessary to obtain a stability estimate for the pressure; without requiring this condition, the pressure would be out of control. The second reason is attributed to the relative importance of the viscous and convective effects in the momentum equation. The stabilized formulation is based on the algebraic variational subgrid scale (SGS) model first introduced in Reference [27]. The variational SGS model first argues that the inability of the mesh to resolve all the flow scales is responsible for the numerical instabilities. Therefore, the model calculates in some approximate way the unresolved scales of the flow, i.e. the scales smaller than the mesh size. The method is extensively described in Reference [28]. Finally, the time discretization is carried out using the generalized trapezoidal rule, i.e. a finite difference scheme. To do so, we consider a partition $0 = t^0 < t^1 < \cdots < t^N = T$ of the time interval $[0, T]$ of interest. The time step is denoted as $\delta t = t^n - t^{n-1}$.

In this work we consider two types of elements using both equal-order interpolation for the velocity and the pressure. The Q1/Q1 element is continuous and bilinear (trilinear in three dimensions) in both velocity and pressure. We will also work with the P1/P1 element, continuous and linear in velocity and pressure. These elements do not satisfy the LBB condition and therefore require the use of stabilization.

A similar numerical model is used to solve the equation for the temperature T, the turbulent viscosity ν_t, and the LSF ψ, which are interpolated like $\mathbf{u}$ and $\mathbf{p}$. They are integrated in time using the generalized trapezoidal rule and the algebraic SGS method is employed to stabilize the possible dominance of convective and reactive terms. See Reference [28] for further details.

3.2. Front advance treatment

In Section 2.4, we mentioned the possibility of identifying the presence and absence of metal by solving a partial differential equation for the LSF. In this work, we propose to solve the partial differential equations in the whole domain Ω, in order to advect the LSF correctly across the interface. We therefore have to define in a clear way the metal domain, the domain of interest. As presented here, the proposed method is exclusive to the finite element method (although it can surely be extended to other methods).

3.2.1. Front definition. Let us take as reference the solution obtained at a time t^n. We assume that the LSF ψ^n is known. The idea is to divide the finite element mesh of Ω into three zones, which are three sets of elements of the finite element discretization: the metal set with elements whose nodes satisfy $\psi > \psi_c$; the foam set with elements whose nodes satisfy $\psi \leqslant \psi_c$; and finally, the front set which includes elements that have both metal and foam nodes, i.e. the remaining elements. In the same way, we define the front nodes as the nodes belonging to front elements, which in addition can be of metal or foam.

Metal nodes are nodes of metal elements; likewise, we define foam nodes similarly. These metal and foam nodes can be of front type also. See Figure 3.

3.2.2. Front advection. The front velocity given by Equations (2) and (6) is imposed as a Dirichlet boundary condition on all the front nodes. This enables to advect the LSF properly across the metal–foam interface, both in the metal and foam domain. Here we must list some

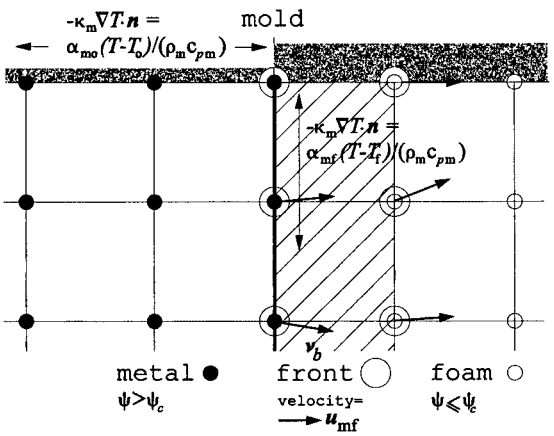

Figure 3. Scheme of the front treatment.

useful numerical ingredients:

- To compute the gradient of the LSF involved in Equation (6), we use a least-square smoothing.
- To obtain a smooth incompressible flow in the foam region, we solve a stationary Stokes problem in the foam set (by setting $v_t = 0$ and removing the time derivative and convection term). In addition, all the boundary nodes of the foam set are left free so that the artificial fluid in the foam can escape the domain and be incompressible. That is, we impose

$$\boldsymbol{\sigma} \cdot \mathbf{n} = 0 \quad 0 \ \Gamma_{\text{fo}} \tag{10}$$

  This step can be understood as an extension of the velocity field in the metal region to foam. It is necessary for the numerical problem (not for the continuous one) since at each time step the front will enter several foam nodes where the velocity needs to be defined.
- To insulate the metal set completely from the foam set, the element matrices of the front set are not assembled in the global stiffness matrix of the RANS, SA and heat equations. Note that for numerical reasons, it is preferable to multiply the front element matrices by a small value (say 10^{-6}) rather than removing them from the assembly. What we have now are two independent domains, one filled with metal, the other filled with foam, and a front of one element width on which the velocity is prescribed to $\mathbf{u}_{\text{mf}}$.
- The velocity vectors of the front nodes located on the mold boundary are projected on the boundary so that the metal does not escape the metal domain as sketched in Figure 3.

3.2.3. Further corrections. As far as the heat equation is concerned, by removing the front element contribution to the stiffness matrix we are implicitly imposing an adiabatic condition for the metal domain, that is $\alpha_{\text{mf}} = 0$ in Equation $(1)_6$. However, if $\alpha_{\text{mf}} \neq 0$, the adiabatic condition can be converted into the desired boundary condition by reconstructing the boundary.

This is explained in Appendix A at the end of the paper. In the independent foam domain, the temperature can be set constant.

3.3. *ALE method with fixed mesh*

When using the level set technique in general casting, involving a metal–air mixture, the Navier–Stokes equations are solved in the entire mold with the physical properties being those of the metal or those of the air according to the value of ψ. The frame of reference is therefore Eulerian. In the present case, the LSF is used to define the metal computational domain, which changes at all times. However, according to the numerical algorithm used to capture the front advance, we want to use the same mesh all along the time integration. So how do we interpret the method described in last section? Figure 4 illustrates the method we propose together with the classical ALE method on a simple one-dimensional example, on the x-axis. The filled bullets represent metal nodes while the empty ones represent foam nodes. Filled bullets with an outer circle indicate metal front nodes. The top line represents the starting solution at time t^n, the metal front node being node 2. If we use an ALE method, as shown in the middle line, nodes 2, 3 and 4 are moved with velocity $u_m = u_m(x)$. In particular, node 2 moves with a velocity $u_m = u_{\mathrm{mf}}$. We recall that when the mesh is moving with velocity $\mathbf{u}_{\mathrm{m}}$, the advection velocity $\mathbf{u}_a$ of the transport equations should be substituted by $\mathbf{u} - \mathbf{u}_m$. Now let us remesh the new configuration so that it coincides with the original mesh. The solution is shown on the third line. We observe that going back to the original mesh, the nodes $2'', 3''$ and $4''$, with co-ordinates $x_{2''} - u_m\delta t$, $x_{3''} - u_m\delta t$, and $x_{4''} - u_m\delta t$, respectively, would fall in the element with nodes 1 and 2. If u_{m} is known, we can therefore find the values of $\mathbf{u}$, T and v_t at time n of the newly metalized nodes. We take for these nodes $u_m = u^{n-1}$. Once we know the position of nodes $1''$, $2''$, $3''$ and $4''$ at time t^n, we can obtain the value of the unknowns by any interpolation procedure at hand. These values are those needed in the time discrete form of the differential equations.

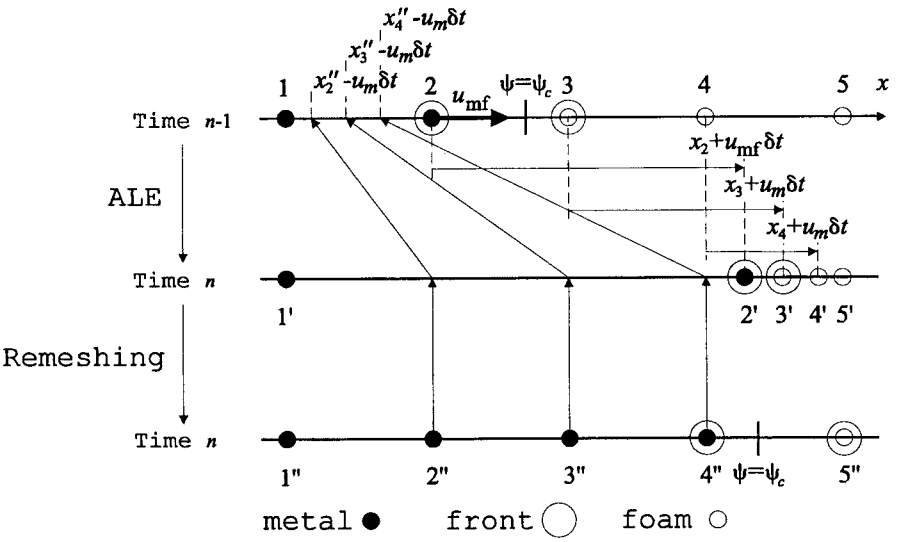

Figure 4. ALE and proposed methods to track front advance.

3.4. Numerical algorithm

We now sum up all the concepts introduced in the previous section. The partial differential equations to solve in Ω are:

$$\begin{aligned}
\partial_t \mathbf{u} + [(\mathbf{u} - \mathbf{u}_m) \cdot \nabla]\mathbf{u} - 2\nabla \cdot [(\nu + \nu_t)\varepsilon(\mathbf{u})] + \nabla p = 0 \\
\nabla \cdot \mathbf{u} = 0 \\
\partial_t \nu_t + (\mathbf{u} - \mathbf{u}_m) \cdot \nabla \nu_t - c_{b_1} S \nu_t - \frac{1}{\sigma}[\nabla \cdot (\nu_t \nabla \nu_t) + c_{b_2}(\nabla \nu_t)^2] + c_{w_1} f_w \frac{{\nu_t}^2}{d^2} = 0 \\
\partial_t T + (\mathbf{u} - \mathbf{u}_m) \cdot \nabla T - \nabla \cdot [(\kappa + \kappa_t)\nabla T] = 0 \\
\frac{\partial \psi}{\partial t} + \mathbf{u} \cdot \nabla \psi = 0
\end{aligned} \tag{11}$$

The turbulent diffusivity coefficient κ_t is given by Equation (7). The physical properties ν and κ, the mesh velocity $\mathbf{u}_m$, and the boundary conditions change with time, according to the position of the front (identified by the value of ψ). Their calculations are presented in Algorithm 1.

Algorithm 1. Numerical algorithm

```
Impose initial conditions, ψ = 1 on the inflow and ψ = 0 elsewhere
Set n = 0
for time steps do
  Set n = n + 1
  Identify the element sets, see Figure 3
  Impose the front velocity (2), (6) as a Dirichlet condition on the front nodes
  Leave free the boundary foam nodes (10)
  Impose the temperature on foam nodes
  Construct the front boundary Γ_mf
  Set ν = ν_i, κ = κ_i where i = m in metal elements and i = f in foam elements
  Let u_m = u^n for newly metalized nodes, and u_m = 0 elsewhere
  Interpolate u^{n-1}, ν_t^{n-1} and T^{n-1} for newly metalized
  nodes of co-ordinates x − u_m δt; see Figure 4
  while stopping criterion not reached do
    Update wall boundary condition for RANS on Γ_mo using wall function approach
    Solve RANS equations (11)_{1,2} in metal and stationary Stokes equations in foam,
    multiplying the contribution of the front elements to the stiffness matrix by 10^{-6}
    Update wall boundary condition for SA on Γ_mo using wall function approach
    Solve SA equation (11)_3, multiplying the contribution of the front elements by 10^{-6}
    Update boundary condition for the temperature on Γ_mf and Γ_mo
    Solve Heat equation (11)_4, multiplying the contribution of the front elements by 10^{-6}
    Solve level-set equation (11)_5
  end while
end for
```

---

4. NUMERICAL EXAMPLES

4.1. Horizontal plate

The first example we solve is the aluminium casting of a two-dimensional plate [3, 16]. The geometry is shown in Figure 5. We consider that the properties of the material do not depend on the temperature. They are shown in Table I. For the sake of simplicity, we set $\alpha_{mo} = 0$ in Equation $(1)_5$ and $\alpha_{mf} = 0$ in Equation $(1)_6$. Note that the Prandtl number of this liquid metal is very small; $Pr = 0.0045$. This means that the diffusion of the temperature is much more efficient than the diffusion of momentum, and therefore the boundary layer

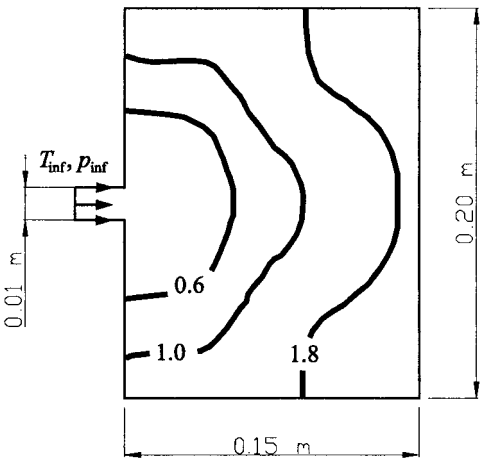

Figure 5. Horizontal plate. Geometry, boundary conditions and experimental front advance [16].

Table I. Horizontal plate. Physical properties and variables in play.

Symbol	Property	Value	
Aluminum			
α_{mf}	Metal to foam heat transfer coefficient	6.00×10^3	(kg/(s^3 K))
ρ_m	Density	2.70×10^3	(kg/m^3)
ν_m	Viscosity	3.70×10^{-7}	(m^2/s)
κ_m	Conductivity	8.32×10^{-5}	(m^2/s)
C_{pm}	Specific heat	8.37×10^2	(J/(kg K))
T_{inf}	Inflow temperature	1.02×10^3	(K)
Foam			
ρ_f	Density	2.00×10^1	(kg/m^3)
c_{pf}	Specific heat	4.00×10^3	(J/(kg K))
E_{mel}	Specific melting heat	8.00×10^2	(J/kg)
E_{vap}	Specific vaporization heat	4.00×10^2	(J/kg)
T_f	Temperature	2.93×10^2	(K)

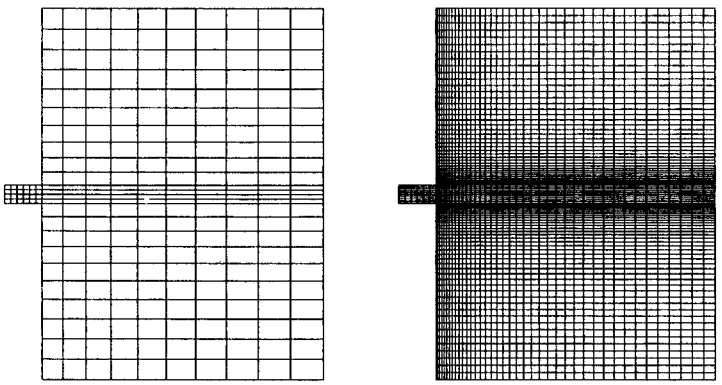

Figure 6. Horizontal plate. (Left) Coarse mesh. (Right) Fine mesh.

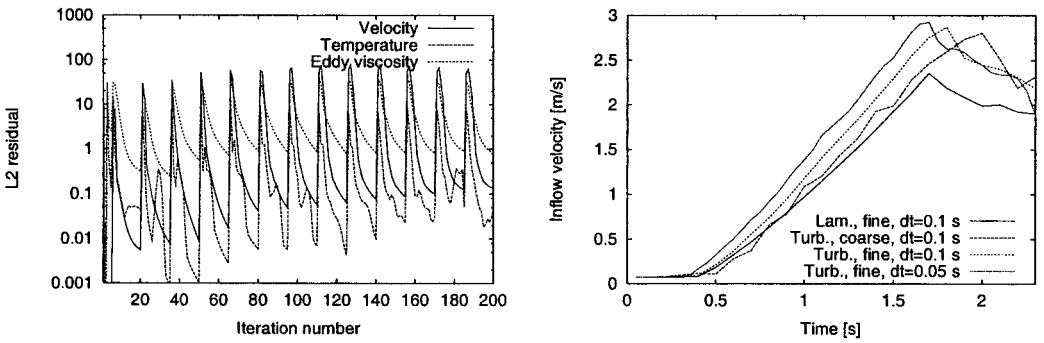

Figure 7. Horizontal plate. (Left) Convergence. (Right) Velocity at inflow.

of the temperature is much larger than that of the velocity. Through the solution of this example we want to test the numerical strategy. We consider the following numerical/physical combinations: laminar and turbulent flows; a fine mesh of 3660 Q1/Q1 elements and a very coarse mesh of 264 elements, see Figure 6; a large time step $\delta t = 0.1$ s and a small one $\delta t = 0.05$ s. In order to take into account the diffusive character of turbulent flows, the laminar simulations are carried out using the RANS equations with a constant eddy viscosity such that $\nu_t = 100\nu$. In the same way, the thermal diffusion is added a constant turbulent diffusion $\kappa_t = \nu_t / Pr_t = 4.35 \times 10^{-5}\,\mathrm{m}^2/\mathrm{s}$. Figure 7 (Left) shows the convergence history of the iterative scheme for the turbulent solution on the fine mesh with $\delta t = 0.1$ s. The velocity residual of the equation falls 4 orders of magnitude in 10 iterations, while the eddy-viscosity residual falls less than 2 orders of magnitude. Figure 7 (Right) compares the evolution of the velocity at the inflow for four different simulations. We note that as the interface evolves, the incoming jet has higher and higher velocities; in fact, the velocity at the front is almost constant, with

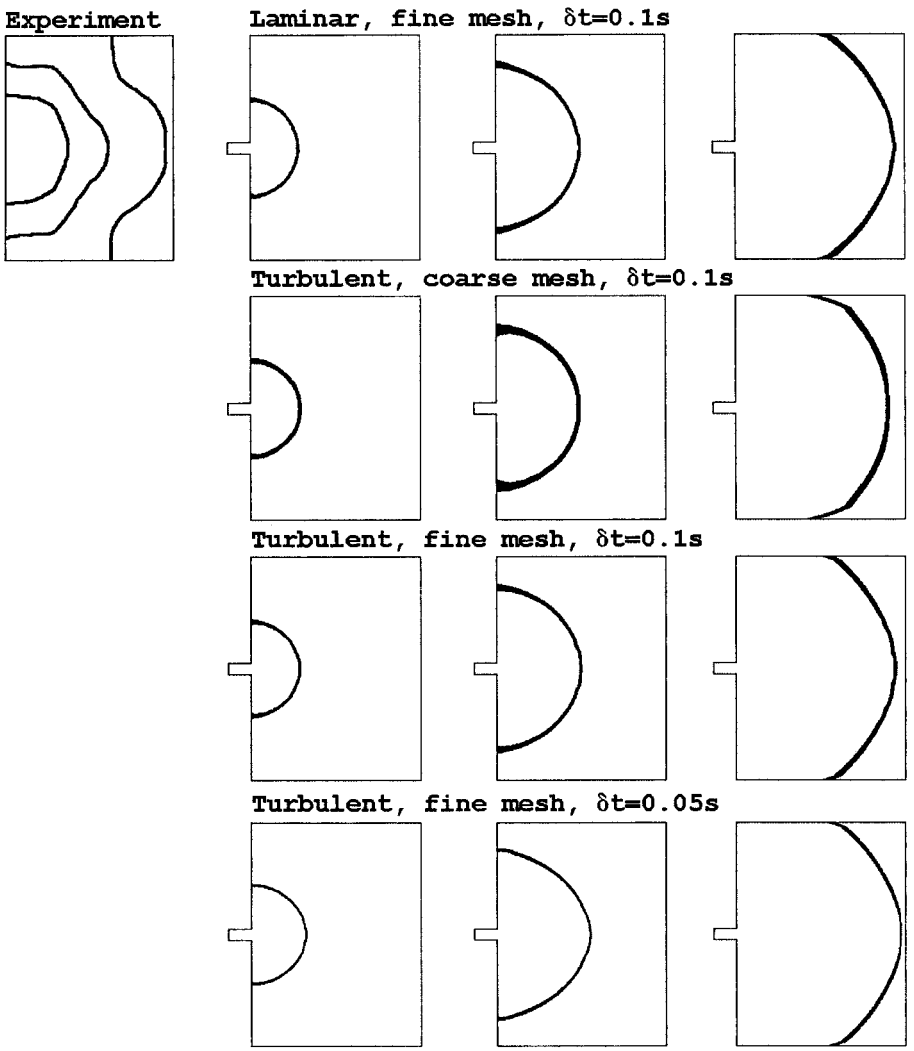

Figure 8. Horizontal plate. Front advance at time 0.6, 1.0 and 1.8 s.

a value of

$$u_{\mathrm{mf}} \approx \frac{\alpha_{\mathrm{mf}}}{\rho_t c_{pf}} = 0.075 \text{ m/s}$$

and as the length of the front increases, the mass flow rate must increase. We observe that the laminar and turbulent solutions obtained on the fine mesh with the same time step give very similar solutions.

Figures 8 and 9 compare the evolutions of the metal front and velocity vectors for the three times shown in Figure 5. Note that for these four simulations the time is set to zero when the front passes the plate entrance. We can observe strong recirculation zones generated once the

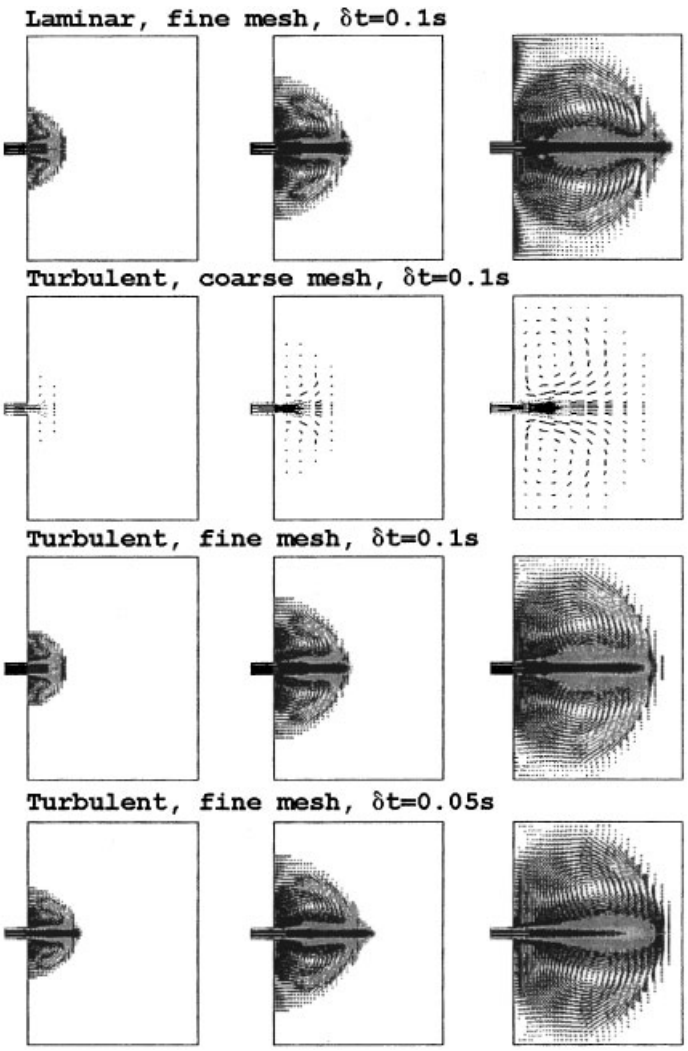

Figure 9. Horizontal plate. Velocity vectors at time 0.6, 1.0 and 1.8 s.

metal enters the plate, and transported by the metal jet from left to right. This recirculation is even captured by the (very) coarse mesh, but located at a different position. We also observe that the distortioned profile of the front obtained in the experiments cannot be well reproduced, although the location of the front is good. This discrepancy could be attributed to many factors, like for example the two-dimensional approximation of the real three-dimensional flow, the fact that the velocity is not normal to the front as we have assumed, the recirculation behind the metal front which may draw some viscous residues along the interface and towards the top and bottom walls and these effects slow down the progression of the metal, etc. The generation of this vortex is shown in more detail is Figure 10. This figure also shows the temperature contours.

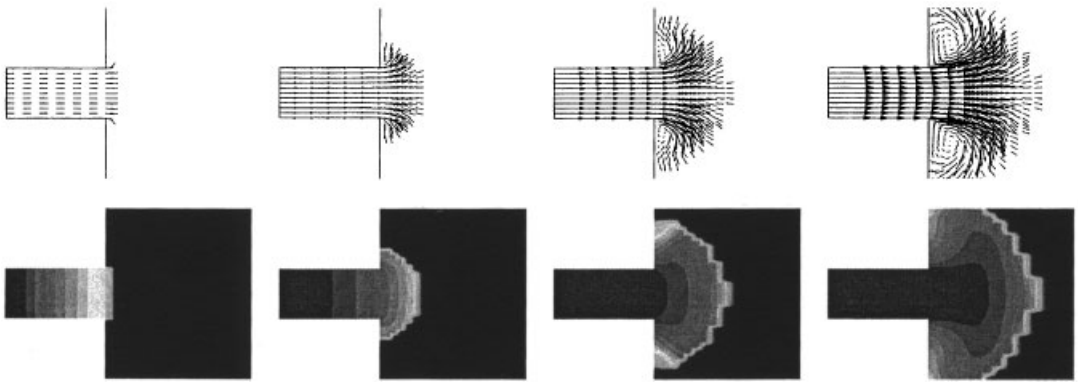

Figure 10. Horizontal plate. Metal entering the plate. (Top) Velocity vectors. (Bot.) Temperature contours.

4.2. Tee shape

We simulate a three-dimensional tee-shaped casting, whose geometry is shown in Figure 11. We take the same physical properties as those of the previous example, and consider laminar flow (augmenting the viscosity and diffusion in the same way). The inner diameter of the vertical cylinder is 0.08 m while the inner diameter of the others is 0.10 m. The geometry is symmetrical with respect to the ingate and therefore the filling should also be symmetric. However, we want to observe the effects of variable foam density. In fact, the foam density is likely to be non-uniform, especially near the injection points. The front velocity model given by Equation (2) is expected to take into account these effects, as the foam density appears in the denominator.

Figure (12) (Top) (Left) shows the different zones of foam density considered in this example, while Figure (12) (Top) (Right) shows the interpolated density contours on the mesh used for this simulation (25344 P1/P1 elements). On the bottom of this figure, we can observe the decrease of the metal advance velocity when it encounters zones of high density. Finally, Figure (13) shows the evolution of the velocity vectors.

5. CONCLUSIONS

We have presented a numerical model to solve lost foam casting problems. This numerical model is based on a finite element method using an ALE formulation with a fixed mesh. It was found that the evolution of the metal domain could be captured well by solving a partial differential equation for a level set function, advected on both sides of the front. The first numerical example showed that the dynamic of the metal was almost exclusively driven by the front advance: the laminar simulation with augmented viscosity and the turbulent simulations gave very similar results. In the second numerical example, we showed that the model for the front velocity could take into account variable foam density. Finally, we give in the appendix some indications on how the physical model could be modified to take into account casting defects.

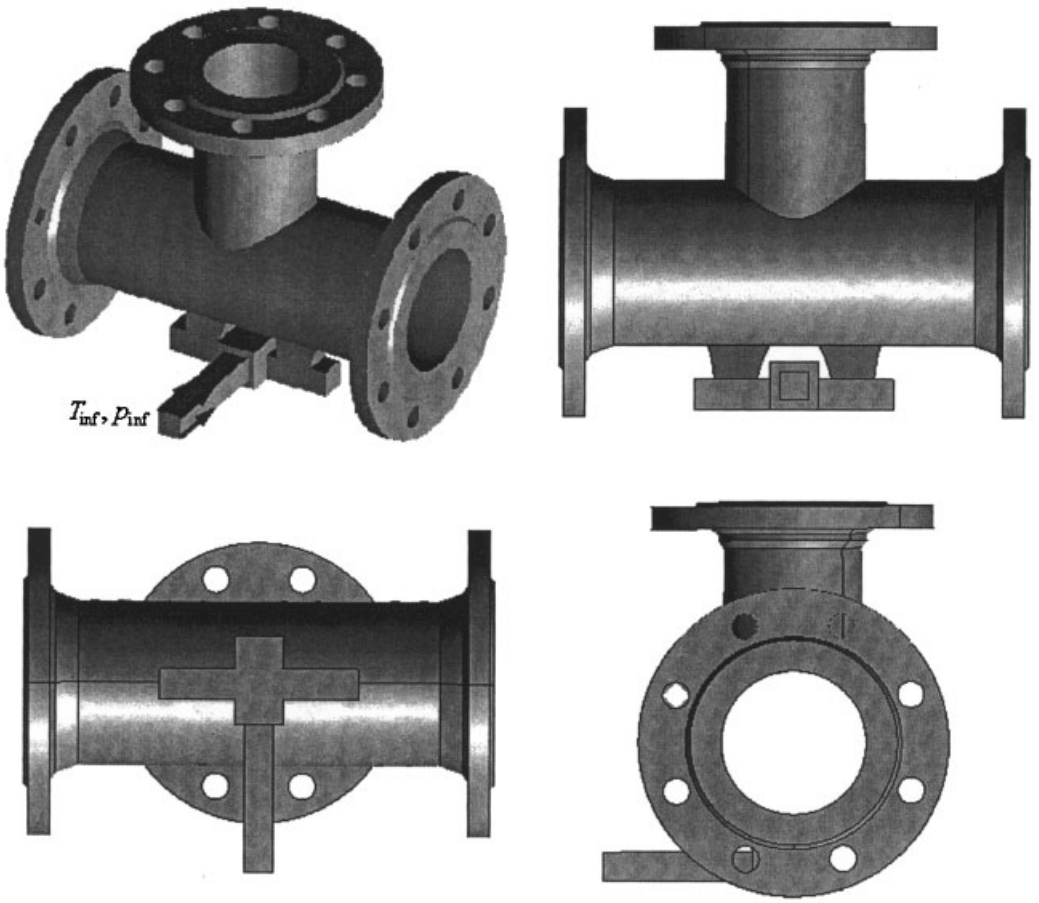

Figure 11. Tee-shape geometry.

APPENDIX A: METAL BOUNDARY RECONSTRUCTION

In Section 3.2.3 we mentioned the possibility of reconstructing at each time step the metal-front boundary. This is useful if a Neumann or Robin condition is to be imposed on the temperature equation.

The algorithm to construct this boundary is given by Algorithm 2.

Algorithm 2. Metal-front boundary reconstruction algorithm

```
for Front elements ielem do
  for Front edges/faces iedge of ielem do
    If all nodes of iedge are of metal, add it to the metal-front boundary
  end for
end for
```

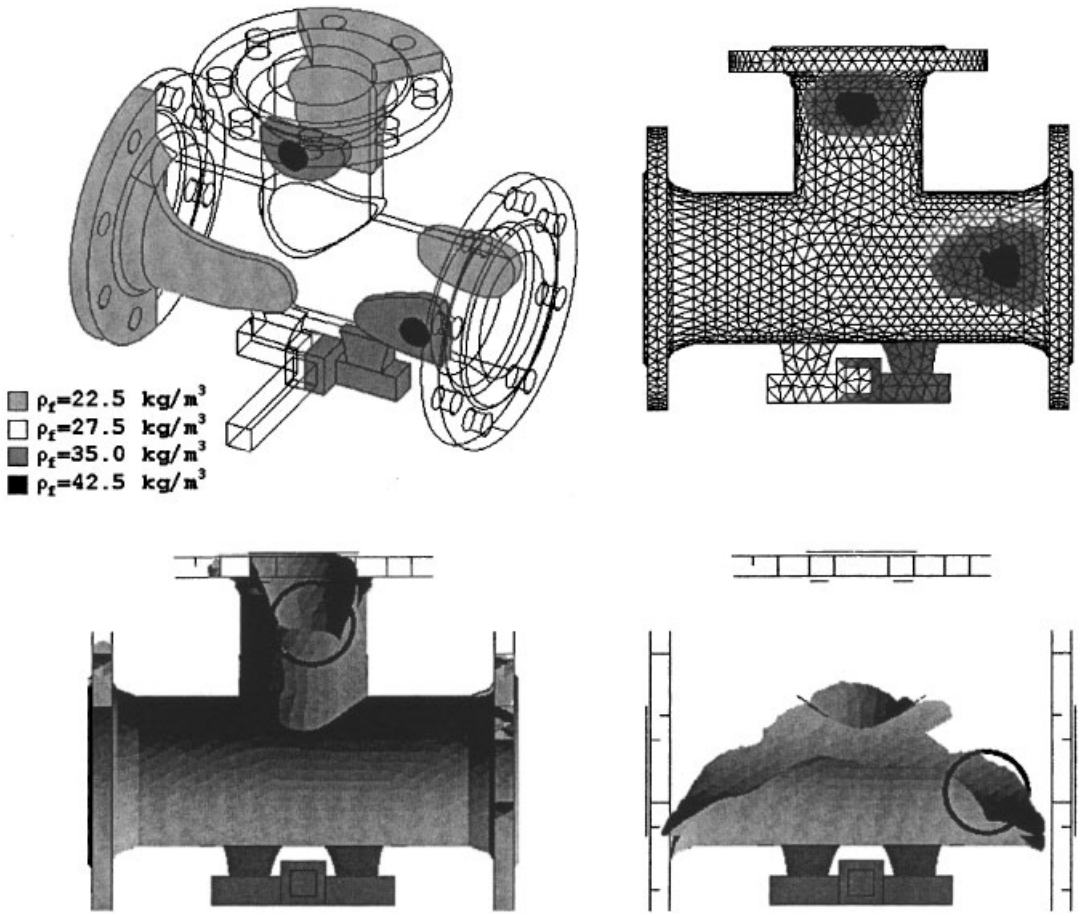

Figure 12. Tee-shape. (Top) (Left) Density zones. (Top) (Right) Mesh and density contours. (Bot.) Metal advance slowed down by high foam density (indicated by the circles).

APPENDIX B: TAKING DEFECTS INTO ACCOUNT

The prediction of defects can be achieved by solving a scalar transport equation for the concentration of residue η of the type

$$\begin{aligned} \partial_t \eta + \mathbf{u}_a \cdot \nabla \eta &= S_\eta \quad \text{in } \Omega_{\mathrm{m}} \\ \eta &= 0 \quad \text{on } \Gamma_{\mathrm{inf}} \end{aligned}$$

where S_η is a source term emanating from the front. As noted in Reference [3], it can be taken to be proportional to the mass of degraded foam.

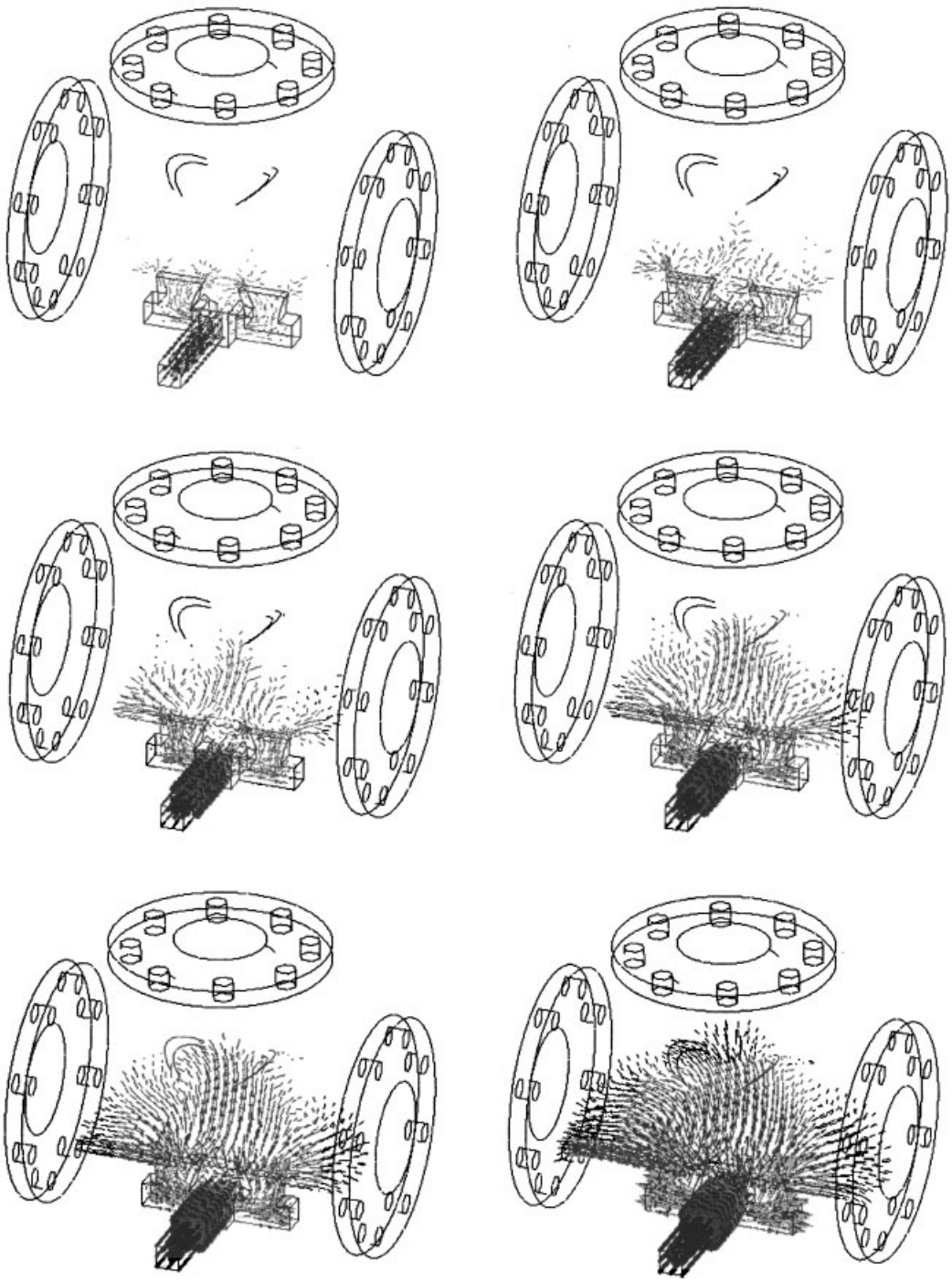

Figure 13. Tee-shape. Velocity vectors along time.

ACKNOWLEDGEMENTS

The authors would like to thank Martin Solina from Quantech ATZ for his work in deleting the millions of lines which appeared during the importation of the CAD files. They also thank Doug Warne and Ian Almond from Saint-Gobain Pipelines for providing the tee-shape geometry. This work was carried out in the framework of the European Project FOAMCAST G1RD-CT-2000-00417.

REFERENCES

1. Piwonka TS. A comparison of lost pattern casting process. *Materials & Design* 1990; **11**(16):283–290.
2. Divone LV. U.S. industrial energy efficiency research, including a focus on metal casting. In *NATO/CCMS Pilot Study. Clean Products and Processes* (*Phase I*), number 238, 1999; 13–15.
3. Hirt CW, Barkhudarov MR. Lost foam casting simulation with defect prediction. In *Modeling of Casting, Welding and Advanced Solidification Process VIII*, Thomas BG, Beckermann C (eds). The Minerals, Metals & Materials Society: San Diego, CA, U.S.A., 1998; 51–57.
4. Kuo J-H, Chen J-C, Pan Y-N, Hwang W-S. Mold filling analysis in lost foam casting process aluminum alloys and its experimental validation. *Materials Transactions* 2003; **44**:2169–2174.
5. Mirbagheri SMH, Varahram N, Davami P. 3D computer simulation of melt flow and heat transfer in the lost foam casting process. *International Journal for Numerical Methods in Engineering* 2003; **58**:723–748.
6. Lewis RW, Ravindran K. Finite element simulation of metal casting. *International Journal for Numerical Methods in Engineering* 2000; **47**:29–59.
7. Muttin F, Coupez T, Bellet M, Chenot JL. Lagrangian finite-element analysis of time-dependent viscous free-surface flow using an automatic remeshing technique application to metal casting flow. *International Journal for Numerical Methods in Engineering* 1993; **36**:2001–2015.
8. Radovitzky R, Ortiz M. Lagrangian finite element analysis of Newtonian fluid flows. *International Journal for Numerical Methods in Engineering* 1998; **43**:607–619.
9. Osher S, Fedkiw R. *Level Set Methods and Dynamic Implicit Surfaces*. Springer: Berlin, 2002.
10. Codina R, Schafer U, Oñate E. Mould filling simulation using finite elements. *International Journal of Numerical Methods for Heat & Fluid Flow* 1994; **4**(3):291–310.
11. Chang RY, Yang WH. Numerical simulation of mold filling in injection molding using a three-dimensional finite volume approach. *International Journal for Numerical Methods in Fluids* 2001; **37**:125–148.
12. Lewis RW, Navti SE, Taylor C. A mixed Lagrangian–Eulerian approach to modelling fluid flow during mould filling. *International Journal for Numerical Methods in Fluids* 1997; **25**:931–952.
13. Gaston L, Kamara A, Bellet M. An arbitrary Lagrangian–Eulerian finite element approach to non-steady state turbulent fluid flow with application to mould filling in casting. *International Journal for Numerical Methods in Fluids* 2000; **34**:341–369.
14. Idelsohn SR, Storti MA, Oñate E. Lagrangian formulations to solve free surface incompressible inviscid fluid flows. *Computer Methods in Applied Mechanics and Engineering* 2001; **191**:583–593.
15. Liu X, Ramsay CW, Askeland DR. Study on mold filling control mechanisms in the epc process. afs 94-148. In *98th AFS Casting Congress*, vol. 102, Hamilton, Ont., Canada, May 1994; 903–914.
16. Yao X, Shivkumar S. Mold filling and solidification in the lost foam process. afs 95-116. In *99th AFS Casting Congress*, Kansas City, Missouri, U.S.A., April 1995; 761–765.
17. Wang C, Ramsay CW, Askeland DR. Effect of processing parameters on mold filling for gray iron epc castings using statistical experimental techniques. afs 94-151. In *98th AFS Casting Congress*, Hamilton, Ont. Canada, May 1994; 921–930.
18. Agelet de Saracibar C. Numerical analysis of coupled thermomechanical frictional contact problems. Computational model and applications. *Archives of Computational Methods in Engineering* 1998; **5**(3):243–301.
19. Houzeaux G, Codina R. Finite element modeling of the lost foam casting process tackling back-pressure effects. In *Proceedings of the ECCOMAS 2004*, *Fourth European Congress on Computational Methods in Applied Science and Engineering*, Jyväskylä, Finland, July 2004, to be published.
20. Scardovelli R, Zaleski S. Direct numerical simulation of free-surface and interfacial flow. *Annual Review of Fluid Mechanics* 1999; **31**:567–603.
21. Spalart PR, Allmaras SR. A one-equation turbulence model for aerodynamic flows, 1992. *AIAA Paper* 92-0439, 1992.
22. Lawn CJ. Turbulent temperature fluctuations in liquid metals. *International Journal of Heat and Mass Transfer* 1977; **20**:1035–1044.
23. Jischa M, Rieke HB. About the prediction of turbulent Prandtl and Schmidt numbers from modeled transport equations. *International Journal of Heat and Mass Transfer* 1979; **22**:1547–1555.
24. Weigand B, Ferguson JR, Crawford ME. An extended Kays and Crawford turbulent Prandtl number model. *International Journal of Heat and Mass Transfer* 1997; **40**(17):4191–4196.

25. Bradshaw PB, Huang PG. The Law of the Wall in turbulent flows. *Proceedings of the Royal Society of London Series* 1995; **451**:165–188.
26. Mohammadi B, Pironneau O. Unsteady separated turbulent flows computation with wall-laws and $k-\varepsilon$ model. *Computer Methods in Applied Mechanics and Engineering* 1997; **148**:393–405.
27. Hughes TJR. Multiscale phenomena: Green's functions, the Dirichlet-to-Neumann formulation, subgrid scale models, bubbles and the origins of stabilized methods. *Computer Methods in Applied Mechanics and Engineering* 1995; **127**:387–401.
28. Codina R. A stabilized finite element method for generalized stationary incompressible flows. *Computer Methods in Applied Mechanics and Engineering* 2001; **190**:2681–2706.

